

Article

Research on the Interaction between the Pile and Shield Machine in the Process of Cutting a Reinforced Concrete Pile Foundation

Xiaoyu Wang ^{1,2,*} and Dajun Yuan ^{1,2}

¹ Key Laboratory of Urban Underground Engineering of the Education Ministry, Beijing Jiaotong University, Beijing 100044, China

² School of Civil Engineering, Beijing Jiaotong University, Beijing 100044, China

* Correspondence: 18115043@bjtu.edu.cn

Abstract: As the urban underground space environment gets more complex, the cases of shield machines encountering and cutting through piles are becoming more common. The interaction between the cutter head and pile foundation directly affects the tunneling performance of the shield machine and the safety of the existing structure. To study the interaction between the pile and the shield machine, a calculation model of the interaction force is established. A field test of cutting two piles was conducted and the rationality of the model is verified by comparing the calculation results with field test data. The model is applied in the project of a shield machine cutting bridge piles in Harbin Metro Line 3, China. The shield operation parameters are predicted and compared with field test results. Besides, the impacts of cutting surface width and eccentric distance on interaction force are discussed. The study shows that there is a significant interaction between the cutter head and the piles when the shield machine cuts reinforced concrete piles, which causes obvious changes in the shield operation parameters and shield performance. The number of tools that are inside the cutting area has a significant effect on the additional torque. The additional torque fluctuates with the rotation of cutter head and increases with the increase of the number of tools. The number of these tools is determined by factors such as the layout of tools in the cutter head, cutting surface width and eccentric distance, which influence the position of each tool relative to the cutting area. As the cutting distance increase, the additional torque of the cutter head shows a trend of first increasing and then decreasing and reaches the maximum value when the cutting distance reaches the radius of the pile. Besides, the additional force and additional moment of the cutter head increase with the increase of the cutting surface width. The impacts of eccentric distance on additional force and additional moment are complicated. The results in this paper can provide reference for similar engineering.

Keywords: shield tunnel; obstacle pile foundation; cut through; interaction force; theoretical model



Citation: Wang, X.; Yuan, D. Research on the Interaction between the Pile and Shield Machine in the Process of Cutting a Reinforced Concrete Pile Foundation. *Appl. Sci.* **2023**, *13*, 245. <https://doi.org/10.3390/app13010245>

Academic Editor: Tiago Miranda

Received: 30 November 2022

Revised: 20 December 2022

Accepted: 22 December 2022

Published: 25 December 2022



Copyright: © 2022 by the authors. Licensee MDPI, Basel, Switzerland. This article is an open access article distributed under the terms and conditions of the Creative Commons Attribution (CC BY) license (<https://creativecommons.org/licenses/by/4.0/>).

1. Introduction

The shield tunneling method has been widely used in urban subway tunnel construction because of its advantages of safety, high efficiency, high degree of mechanization and little influence on the surrounding environment. With the rapid development of urban subway construction and the increasing density of the subway network, it is common for newly built shield tunnels to encounter the pile foundation of the existing structures [1–4]. When reinforced concrete piles foundation directly intrudes into the tunnel boundary, it causes great difficulties in tunnel construction. Generally, traditional methods such as demolishing the original building (structure), pulling out piles from the ground and digging piles after excavating the shaft are used to remove the pile in advance. Although these methods are relatively safe and mature, they also have disadvantages, such as large impacts on the surrounding environment, high cost and long construction period [5–8].

In recent years, cases of shield machines directly cutting through reinforced concrete piles have appeared frequently, especially in China. In the construction of Tel Aviv Light Rail Red Line in Israel, the TBM (Tunnel Boring Machine) cut and passed through 14 reinforced concrete piles [9]. A shield tunnel crosses through group pile foundation of a road bridge with pile underpinning technologies in Shanghai, China [10]. Some other similar cases also appeared in a few cities in China, such as Guangzhou and Shenzhen. It is crucial to carry out research related to reinforced concrete pile cutting technology.

At present, most studies focus on the influence of tunnel excavation on pile foundation and the influence of pile on the structure of tunnel in projects where the tunnels pass by nearby piles. A variety of papers have been conducted on this subject based on theoretical analyses [11–17], numerical approaches [18–23] and laboratory model tests [24–32]. However, few studies have focused on the problem of shield machines directly cutting reinforced concrete piles. Deng et al. studied a new type of polycrystalline diamond compact cutter, which is based on cutters widely used in oil drilling, to cut reinforced concrete [33]. S.W. Lee investigated the behavior of piles in a large pile group and associated buildings through 3D finite element analysis and parametric studies. A field test study and the practice of cutting piles in Suzhou subway construction were conducted by Yuan et al. [34] and Wang et al. [35]. Besides, the interaction between the cutter head and pile directly affects the tunneling performance of shield machine and little research has been done on this issue.

A theoretical model is established to study the interaction force between the shield machine cutter head and piles. A field test of cutting two piles was conducted and the rationality of the model is verified by comparing the calculated results with field test results. The model is applied in the project of a shield machine cutting bridge piles in Harbin Metro Line 3, China. The shield operation parameters are predicted and compared with field test results. Besides, the impacts of cutting surface width and eccentric distance on interaction force are discussed.

2. Project Overview

The project of shield machine cutting bridge piles in Harbin Metro Line 3 is located in interval between Hesong Street station and Gongludaqiao station, which is in the central area of Harbin city in China. According to the construction plan, the interval tunnel from Hesong Street station to Gongludaqiao station has to cut and pass through the reinforced concrete pile foundation of Qianjinlu Bridge, as shown in Figure 1.

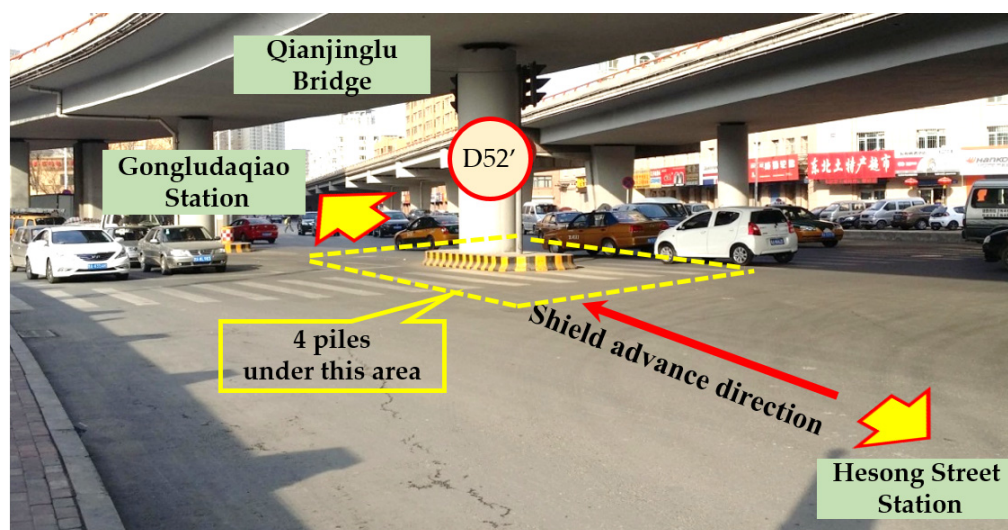


Figure 1. Plan of the project.

In the section of crossing the bridge piles, the tunnel is stacked up and down, and the vertical net distance is 4.5 m. The lower tunnel is constructed first and then the upper

tunnel is constructed. Each tunnel is 6.0 m in outer diameter and 5.4 m in inner diameter. The tunnels are constructed with precast segments, and the length of each segment is 1.2 m. Three piles are scheduled to be cut by the shield machine in construction and one pile is passed by. The piles have a diameter of 1.2 m, a length of 33 m and are built of C25 concrete. The measure of pile foundation underpinning has been taken to ensure the safety and normal use of the bridge before cutting the piles. The main stratum in the excavation range of the tunnel is medium sand and silty clay layers. The soil mass surrounding the foundation of Qianjinglu Bridge is mainly composed of medium sand and silty clay layers. Starting from the surface, the soil layers are miscellaneous fill ①₁, fine sand layer ②₃, medium sand layer ⑦₂, silty clay layer ②₄, medium sand layer ⑦₂, silty clay layer ⑦₁ and medium sand layer ⑦₂. The water table is about 4.8 m from the surface and is in the medium sand layer ②₃. The basic physical and mechanical soil properties are shown in Table 1. The relative position of the piles and tunnels is shown in Figure 2.

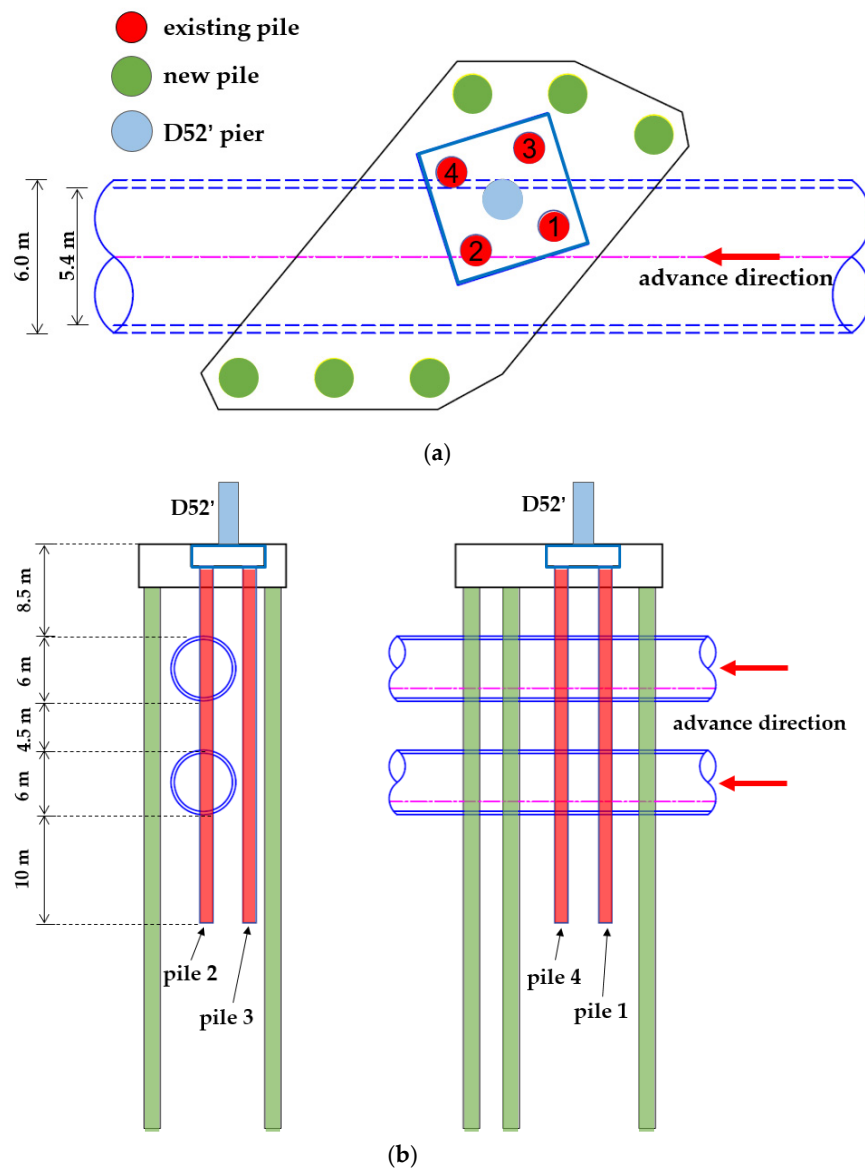
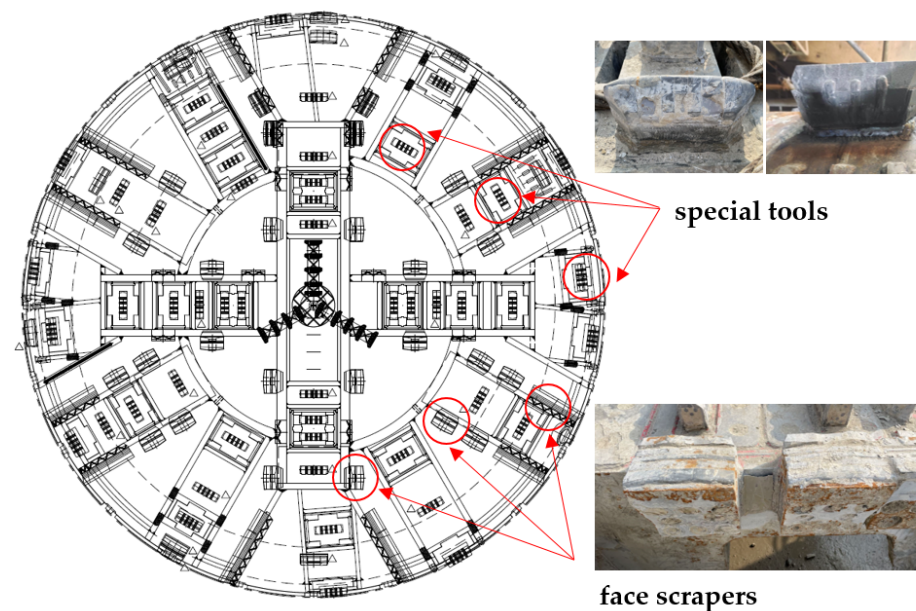


Figure 2. The relative position of tunnels and piles: (a) Top view; (b) Front view and side view.

Table 1. Physical and mechanical parameters of each soil layer.

Layer	Thickness (m)	Density ρ (g/cm ³)	Cohesion c (kPa)	Friction Angle φ (°)
① ₁	3.0	-	-	-
② ₃	5.6	1.98	0	28.5
⑦ ₂	3.1	2.08	0	33.8
② ₄	4.0	1.93	28.9	20.6
⑦ ₂	9.9	2.08	0	33.8
⑦ ₁	4.2	1.94	32.5	19.9
⑦ ₂	12.3	2.08	0	33.8

A slurry balance shield machine manufactured by CCCC Tianhe Machinery and Equipment Manufacturing Co., Ltd., Changshu city, China was used in tunneling. The shield machine with a cutter head diameter of 6270 mm is equipped with 60 modified shell-shaped tools (special tools) to efficiently cut reinforced concrete piles. The cutter head and cutter layout are shown in Figure 3.

**Figure 3.** Cutter head and layout of tools.

3. Calculation Model

Because of the high strength of reinforced concrete piles, shield machines used to cut piles are usually equipped with special tools which are designed and modified to remove reinforced concrete efficiently. The height of the special tools is a bit higher than that of the face scrapers in order to protect the face scrapers. The shield machine mainly relies on these special tools to cut reinforced concrete and the face scrapers rarely directly contact the piles. Therefore, the force of the shield machine applied on the piles is mainly the comprehensive result of the penetration force and cutting force of the special tools.

A theoretical calculation model is established to study the interaction force between the shield machine cutter head and piles. Because the diameter of piles is much smaller than the cutter head diameter in most circumstances, only a few parts of the tools are in the state of cutting pile at a certain time. Furthermore, tools in different positions have different effects on piles. Therefore, it is necessary to determine before the calculation which tools are in the state of cutting and which tools are not.

The Cartesian coordinate system is established as shown in Figure 4. Take the center of the cutter head as the coordinate origin. The right direction is the positive direction of

the x-axis, and the upward direction is the positive direction of the y-axis. Set the z-axis positive direction as the advancing direction of the shield machine.

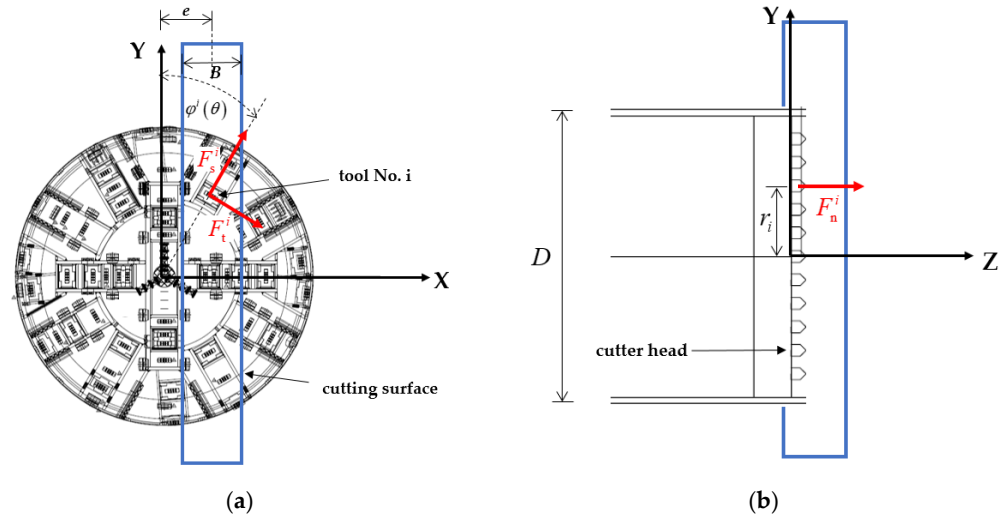


Figure 4. Schematic diagram of calculation model: (a) Front view; (b) Side view.

Suppose that the cutter head rotates clockwise around the center and i is the tool number, then the tools which are cutting pile at a certain time can be determined by the following method. Define the tool phase angle φ as the angle across which the positive half axis of y axis rotates clockwise to the tool center. The initial phase angle (when $\theta = 0$) of tool No. i is φ_0^i ($0 \leq \varphi_0^i \leq 2\pi$). Then, the phase angle of tool No. i at any time can be written as:

$$\varphi^i(\theta) = \varphi_0^i + \theta \tag{1}$$

Then:

$$\begin{cases} i \in W_\theta, \text{ only if } e - \frac{B}{2} \leq r_i \cdot \sin \varphi^i(\theta) \leq e + \frac{B}{2} \\ i \notin W_\theta, \text{ if } r_i \cdot \sin \varphi^i(\theta) < e - \frac{B}{2} \text{ or } r_i \cdot \sin \varphi^i(\theta) > e + \frac{B}{2} \end{cases} \tag{2}$$

where θ is the rotation angle of the cutter head; W_θ is the number set of all the tools that are in contact with the pile when the rotation angle is θ ; e (eccentric distance) is the distance between the pile central axis and the cutter head center; B (cutting surface with) is the width of contact surface between the cutter head and the pile; r_i is the radius of cutting path of the tool No. i .

The force exerted by the cutter head on the pile is the vector sum of the forces exerted by each cutter on the pile. Therefore, the total forces and total moments of the cutter head on pile can be calculated by Equations (3) and (4):

$$\begin{cases} F_x(\theta) = \sum_{i \in W_\theta} F_t^i \cdot \cos \varphi^i(\theta) \\ F_y(\theta) = - \sum_{i \in W_\theta} F_t^i \cdot \sin \varphi^i(\theta) \\ F_z(\theta) = \sum_{i \in W_\theta} F_n^i \end{cases} \tag{3}$$

$$\begin{cases} M_x(\theta) = - \sum_{i \in W_\theta} F_n^i \cdot r_i \cdot \cos \varphi^i(\theta) \\ M_y(\theta) = \sum_{i \in W_\theta} F_n^i \cdot r_i \cdot \sin \varphi^i(\theta) \\ M_z(\theta) = \sum_{i \in W_\theta} F_t^i \cdot r_i \end{cases} \tag{4}$$

where F_x, F_y, F_z are the total forces of the cutter head on the pile in the x, y, z direction, respectively; M_x, M_y, M_z are the total moments of cutter head on the pile in x, y, z direction, respectively; F_n^i is the penetration force of tool No. i ; F_t^i is the cutting force of tool No. i .

In the above model, the force exerted by tools on reinforced concrete is decomposed into penetration force F_n^i , cutting force F_t^i and side force F_s^i . The side force is usually very small and is not considered in the model. In addition, due to the short and uncertain contact time between the tools and the steel bar, the contact force between the tool and steel bar is ignored in order to simplify the model. Moreover, the additional loads of the cutter head caused by the cutting pile and the force applied on the pile by cutter head have the same magnitude and opposite direction according to Newton's third law. Therefore, F_z and M_z can be considered the additional thrust and additional torque of the shield machine, which are crucial to the setting of shield operation parameters. F_x, F_y, M_x, M_y are unbalanced forces and unbalanced moments of cutter head which can have an impact on the control of shield attitude.

It should also be noted that the force and moment calculated by the above model are the additional force caused by the interaction between the pile and the concrete, which is part of all the loads on the cutter head, except for the loads from other surrounding strata.

In addition, the thrust and torque are two of the most important shield advancing parameters that influence the performance of excavation in the actual construction. Compared with these two parameters, the unbalanced force and unbalanced moment are generally small. The shield machine body is strongly restrained by the surrounding strata in the radial direction of the cutter head. Hence, unbalanced forces and moments of shield machine caused by pile cutting have relatively little effect on shield tunneling performance. The following section of this paper mainly focuses on the analysis and discussion of the influence of the interaction between the cutter head and the pile foundation on the thrust and torque.

4. Model Verification

4.1. Cutting Force of a Single Tool

Before calculating the resultant force and moment caused by pile cutting, it is necessary to obtain the force of cutting concrete with a single tool. Many studies have been carried out on this issue and cutting force in different condition was investigated through numerical simulation and laboratory test [36–38]. The cutting force of a single tool cutting concrete is mainly affected by tool parameters (such as blade width, edge angle, rack angle and relief angle), strength of concrete and movement parameters (such as penetration and cutting speed). The selection of the geometric parameters of the shield tools usually takes into account the construction stratum conditions, cutting efficiency, wear resistance, etc., and it is hard to change once the tools were finished. The effect of the variation of the cutting speed under normal construction conditions on the cutting force is not obvious. Therefore, this paper focuses on the calculation of cutting force with different penetration.

A numerical simulation model of a single tool cutting concrete was established based on finite element software LS-DYNA. The Holmquist-Johnson-Cook (HJC) model is introduced to simulate the failure of concrete material [39] and modified HJC model parameters are used according to the results of laboratory tests. The HJC model is a constitutive model widely applied to the numerical simulations of the dynamic responses of concrete-like materials. The comprehensively considers strain rate effect, damage evolution effect, confining pressure effect, crushing effect and pressing effect. The concrete cutting process by shield tool is a process of concrete damage, crushing and destruction caused by dynamic penetration. Therefore, HJC model is considered suitable in the numerical calculation of cutting force in concrete materials.

The model mainly consists of three parts: strength model, damage evolution model and state equation.

- (1) The material strength model is described by the normalized equivalent stress, as in Equation (5) and Figure 5a:

$$\sigma_{eq}^* = [A(1 - D) + B(p^*)^N](1 + \ln \dot{\epsilon}^*) \tag{5}$$

where $\sigma_{eq}^* = \sigma_{eq}/f_c$ is the normalized equivalent stress; σ_{eq} denotes the actual equivalent stress; S_{FMAX} is the normalized maximum strength that the concrete material can withstand and $\sigma_{eq} \leq S_{FMAX}$; f_c is the unconfined uniaxial compressive strength; $p^* = p/f_c$ is the normalized pressure, where p is the actual pressure; $\dot{\epsilon}^* = \dot{\epsilon}/\dot{\epsilon}_0$ is the dimensionless strain rate; $T^* = T/f_c$ is the normalized tensile strength, where T is the unconfined uniaxial tensile strength; A, B and N are material constants which represent the normalized cohesive strength, the normalized pressure hardening coefficient and the pressure hardening exponent, respectively; C is the strain rate coefficient; D ($0 \leq D \leq 1$) is the accumulated damage.

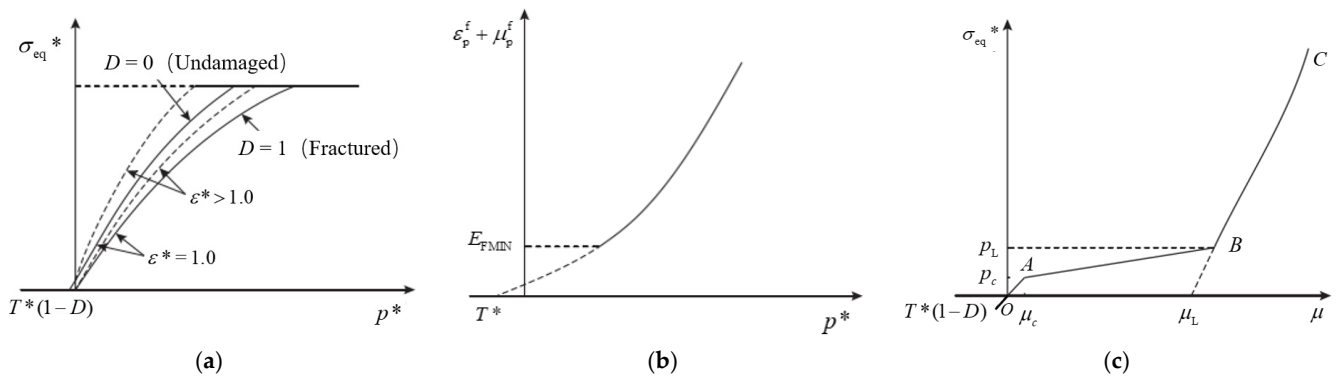


Figure 5. HJC model: (a) Strength model; (b) Damage of HJC model; (c) Equation of state.

(2) Damage of the HJC model is accumulated from both the equivalent plastic strain and plastic volumetric strain, as in Equation (6) and Figure 5b:

$$D = \frac{\Delta\epsilon_p + \Delta\mu_p}{\epsilon_p^f + \mu_p^f} \tag{6}$$

$$\epsilon_p^f + \mu_p^f = D_1(p^* + T^*)^{D_2} \geq E_{FMIN} \tag{7}$$

where $\Delta\epsilon_p$ and $\Delta\mu_p$ are the effective plastic strain increment and plastic volumetric strain during a cycle of integration, respectively; $\epsilon_p^f + \mu_p^f$ is the total plastic strain under a constant pressure until fracture; D_1 and D_2 are the damage constants; E_{FMIN} is the minimum strain.

(3) The relationship between the volume strain and actual pressure in the HJC model is expressed through equation of state and separated into three phases, as shown in Figure 5c. The first phase (OA) is linear elastic and expressed as follows:

$$p = K\mu; \quad p \leq p_c, \mu \leq \mu_c \tag{8}$$

where $K = p_c/\mu_c$ is the elastic bulk modulus; p_c elastic limit pressure; μ_c is the elastic limit volumetric strain.

In the second phase (AB), the void inside the material is gradually compressed and the plastic volumetric strain appears.

$$p = p_c + K_1(\mu - \mu_c); \quad p \leq p_1, \mu \leq \mu_1 \tag{9}$$

where $K_1 = (p_1 - p_c)/(\mu_1 - \mu_c)$ is the slope.

In the third phase (BC), the void inside the material disappears and the material is completely compacted.

$$p = K_1\bar{\mu} + K_2\bar{\mu}^2 + K_3\bar{\mu}^3 \tag{10}$$

where K_1, K_2 and K_3 are the material constants; the modified volumetric strain is $\bar{\mu} = (\mu - \mu_L)/(1 + \mu_L)$; μ_L is the grain density of the material.

Appropriate model parameters are critical to the accuracy of cutting force calculations. Many scholars have fitted the parameters of the HJC model and given the results. The parameters of the HJC model below are determined based on the available static and modified according to laboratory dynamic test data [40]. The tool parameters are based on the special tools used in the field test and engineering practice case below. The blade width of the special tools in the model is 4 mm, the edge angle is 90 degrees, the rake angle is -45 degrees and the relief angle is 0 degrees. These are common parameter values for special tools (shell-shaped tools) used for cutting reinforced concrete piles. In consideration of computational efficiency and accuracy, the unit size ratio between the cutting area and other areas should be reasonably adjusted. The size of the concrete unit inside the cutting area is about 0.1 mm. The cutter model is set as a rigid body. The parameters of the HJC model are shown in Table 2. The diagram of model and an example of cutting process are shown in Figure 6.

Table 2. Parameters for the HJC model.

Strength Parameters				Damage Parameters		
<i>A</i>	<i>B</i>	<i>N</i>	<i>S_{FMAX}</i>	<i>D₁</i>	<i>D₂</i>	<i>E_{FMIN}</i>
0.27	1.5	0.87	20	0.04	1.0	0.01
Equation of State Parameters						
<i>p₁</i> (GPa)	<i>p_c</i> (GPa)	<i>μ₁</i>	<i>μ_c</i>	<i>K₁</i> (GPa)	<i>K₂</i> (GPa)	<i>K₃</i> (GPa)
1.780	0.008	0.16	7×10^{-4}	9.23	141.24	136.50
Basic Parameters				Strain Rate		
<i>ρ</i> (kg/m ³)	<i>G</i> (MPa)	<i>T</i> (MPa)	<i>f_c</i> (MPa)	<i>C</i>		
2110	8750	1.62	24.45	0.012		

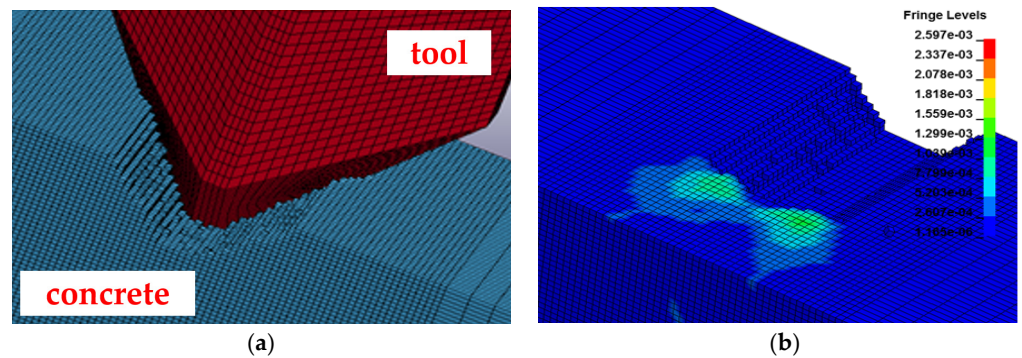


Figure 6. The 3D numerical model of cutting concrete: (a) Diagram of model; (b) Equivalent stress diagram of the concrete.

In order to facilitate the calculation of the following engineering cases in this paper, the cutting force with different penetration was obtained through this model. The results are shown in Figure 7. It can be seen that the relation between cutting force and penetration is nearly linear and the cutting force is also linearly related to the penetration.

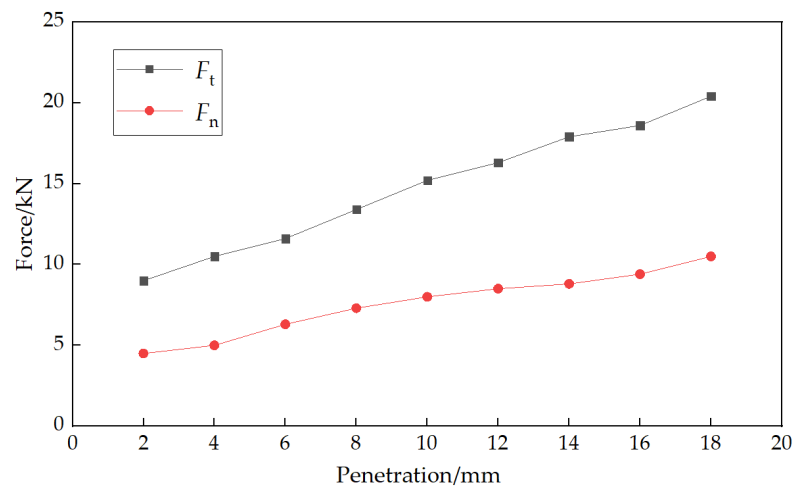


Figure 7. Cutting force and penetration force under different penetrations.

4.2. Field Test of Cutting Piles

In order to observe and study the process of shield machine cutting reinforced concrete piles, a field test of cutting two piles was conducted earlier in Suzhou, China. Shield operational parameters, such as the total thrust force, the total torque, the cutter head rotation and the advance rate, were collected in the process of cutting. The data were processed and compared with the results from the calculation model to judge the accuracy of the calculation model. Considering the feasibility, safety and economy of the test, two test piles were cast in front of the tunnel portal as in Figure 8. The layout of the test piles is shown in Figure 9. The pile A is arranged at the centerline of the portal and the pile B pile is 1.8 m away from the axis of the tunnel. The longitudinal offset between the two piles was 0.3 m. Twenty main bars of $\phi 22$ and HRB 335 were installed in each pile. The concrete strength is C30 and the thickness of concrete protective layer of piles is 50 mm. The top and bottom of the test piles were fixed by means of welding and planting bars, which can prevent the pile from moving back and forth during the cutting.

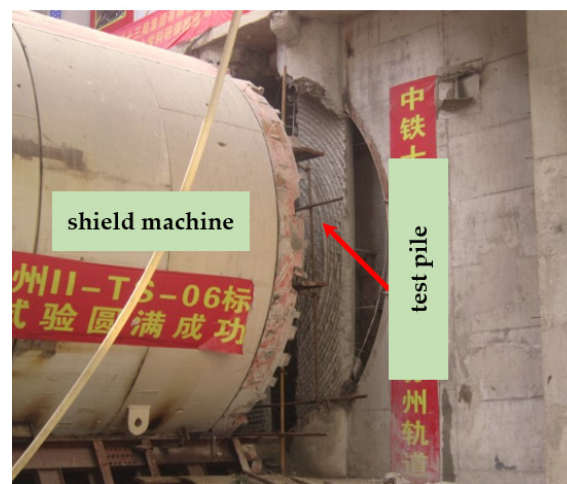


Figure 8. Photo of the field test site.

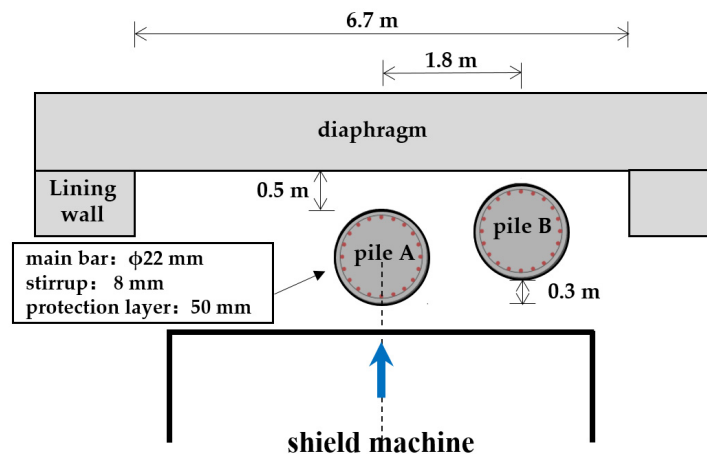


Figure 9. The layout of the test piles.

The cutting process is divided into five stages according to different cutting conditions and advancing parameters, which are shown in Figure 10. The advance distance is 150 mm, 150 mm, 180 mm, 230 mm and 300 mm, respectively. Shield operation parameters in different stages are listed in Table 3.

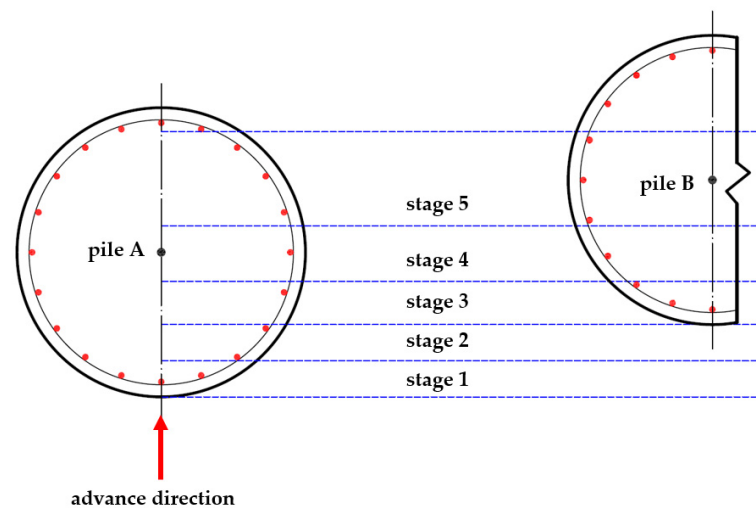


Figure 10. Divided stages of the field test.

Table 3. Shield operation parameters in different stages.

Stage	Distance (mm)	Advance Rate (mm/min)		Rotation Rate (rpm)	Rotation Direction	Thrust (kN)	
		Maximum	Average			Maximum	Average
1	150	8	1.88	0.8	counter-clockwise	1140	997.0
2	150	8	3.44	0.5, 0.8, 1.0	counter-clockwise	1450	1220.5
3	180	7	1.29	0.5	clockwise	1590	1199.6
4	230	6	1.68	0.8	clockwise	1770	1446.8
5	300	8	3.11	0.8	clockwise	1760	1254.6

4.3. Comparison of the Interaction Force

The shield operation parameters obtained from field tests were processed and compared with the results from calculation mode. Some of important shield operation parameters include the total thrust, the total torque, the cutter head rotation rate, the advance rate, etc. Among them, the total thrust and the cutter head rotation rate are active control

parameters, while the total torque and the advance rate are passive parameters, which are produced by different shield machine monitors and change with difference of geological conditions and excavation environment. Therefore, the four shield operation parameters are correlated with each other. These parameters reflect the interaction of the shield machine with the piles.

Before starting pile cutting, the thrust and torque of the shield machine in non-cutting pile state were tested. When the shield machine was advancing at a speed of 1~10 mm/min on the guide rail bracket, the total thrust was nearly steady at about 900 kN and the total torque was about 400 kN·m. The additional torque values of the cutter head at the starting position, midpoint position and end position of each stage were calculated and compared with field test results. Since in this test, the shield is in an open space and there is no influence of the surrounding ground environment, the total torque and total thrust of the cutter head can be obtained by adding the above two loads. In addition, penetration depth in the numerical model refers to the vertical depth from the blade edge to the cutting surface. In the field test, the penetration depth of the tools is not constant during the advance of the shield machine because the advance rate fluctuates continuously. Penetration in shield tunneling is usually calculated by dividing the advance rate by the rotation rate and it represents the advance distance of the shield machine within one revolution of the cutter head. It is a simplified approximate calculation of the true penetration of the tools and was widely used in engineering. The steadier the advance rate is, the closer the calculated penetration is to the real penetration depth of the tools. When performing model calculations, the penetration is calculated using the average advance rate for a period of time around the calculation cross-section. Calculated total torques are compared with field test results. As shown in Figure 11, the field test torque fluctuates obviously as the shield machine continues to advance. In the first and second stages, the torque increases slightly. At these two stages, the cutter head only cuts pile A and has not touched pile B. From the third stage, the torque began to increase significantly. The main reason is that the cutting condition has changed from cutting one pile to cutting two piles at the same time, which means more shield tools are involved in cutting piles. In the fourth stage and the early stage of the fifth stage, the shield torque has been at a high value of about 1300 kN·m and the cutting surface width of the two piles is close to the diameter of the piles. The field test torque reached a peak of 1768 kN·m at the end of the fourth stage and the calculated result also reached a peak of 1396 kN·m at the same position. Subsequently, at the end of the fifth stage, the cutting force of the cutter head decreased rapidly and the top of pile A was broken. Despite there being certain differences between the field test data and the calculated results, overall, the calculated torque is roughly consistent with the field test data. To some extent, this verifies that the additional torque by calculation model is reasonable.

It should be noted that the total thrust of the shield machine is an active parameter by the shield machine operator. The penetration force exerted by the cutter head on the pile changes when the shield machine operator adjusts the value of the total thrust. The penetration force calculated by the model refers to the thrust applied on the pile to satisfy the cutting of the piles during normal tunneling. In actual excavation, it is usual to actively increase the total thrust to ensure the ability to cut piles. At the same time, the advance rate and the penetration of the shield also change accordingly. The contacting state between the tools and the piles changes and the total torque changes as well. In this field test, the shield thrust is dynamically adjusted according to the advance rate to ensure the smooth cutting of piles. Therefore, the measured shield thrust is greater than the theoretical calculation of the minimum thrust force needed to complete the cutting.

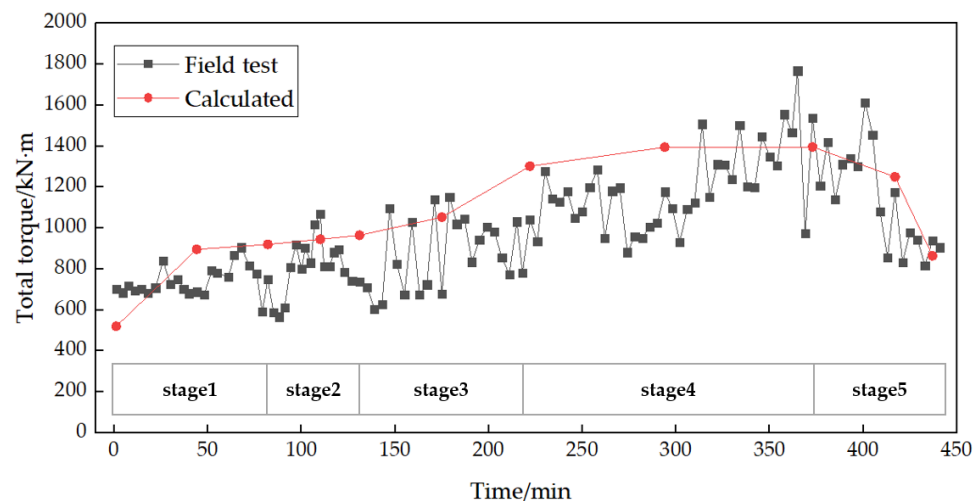


Figure 11. Total torque at each cutting stage.

5. Engineering Practice

For the piles in the project of cutting bridge piles in Harbin Metro Line 3, the additional torque during the pile cutting process was predicted based on the established calculation model. The calculated results were compared with the field test data in the process of construction. The field test additional torque is obtained by subtracting the average value of the total torque within a ring of segment before the pile cutting from the total torque when the pile is cut by the shield machine. The variation of additional torques under the two conditions of cutting pile No. 1 and pile No. 2 are given below. The piles have a diameter of 1.2 m. The eccentric distances of pile No. 1 and pile No. 2 are -1209 mm ($0.2 D$) and -250 mm (nearly 0), respectively. The cutter head rotation rate is 1.1 rpm and the advance rate fluctuates with an average value of about 8 mm/min.

5.1. Additional Torque at Different Rotation Angles

Figure 12 shows additional torque at different rotation angles of cutter head when cutting through pile No. 1. It can be seen from the figure that both the field test additional torque and calculated results fluctuate obviously with the rotation of cutter head. The field test additional torque varies in a range from 240 kN·m to 533 kN·m, with an average value of 331 kN·m. The calculated result varies in a range from 191 kN·m to 486 kN·m, with an average value of 404 kN·m. A main reason for the fluctuation of additional torque is the number of tools that are in contact with the pile. Besides, the state of contact between the cutter head and pile is complicated and uncertain in excavation process, which can cause some data errors as well. Overall, the calculated additional torque is roughly consistent with the field test data in construction. To some extent, this verifies that the prediction of the additional torque by the calculation model is reasonable.

Figure 13 shows additional torque at different rotation angles of cutter head when cutting through pile No. 2. Similar to Figure 12, field test additional torque and calculated results fluctuate with the rotation of cutter head. The field test additional torque varies from 317 kN·m to 794 kN·m, with an average value of 525 kN·m. The calculated result varies from 295 kN·m to 685 kN·m, with an average value of 440 kN·m. It is noticeable that the variation of additional torque in Figure 13 is a bit different from that in Figure 12. There are four obvious peaks in both the calculated and the field test results (0 degrees and 360 degrees are considered same rotation angle). The positions of the four peaks are about 0 degree, 90 degrees, 180 degrees and 270 degrees, corresponding to the four positions where the tools are arranged most. This suggests that when designing the layout of the tools on the cutter head, the tools should be distributed as evenly as possible, which can reduce large torque fluctuations. In addition, the average additional torque value in Figure 13 is greater than that in Figure 12. A reason is that the cutting surface width in Figure 13 is

greater and eccentric distance is smaller, which leads to a lower cutting area and a lower number of tools that are in contact with the pile.

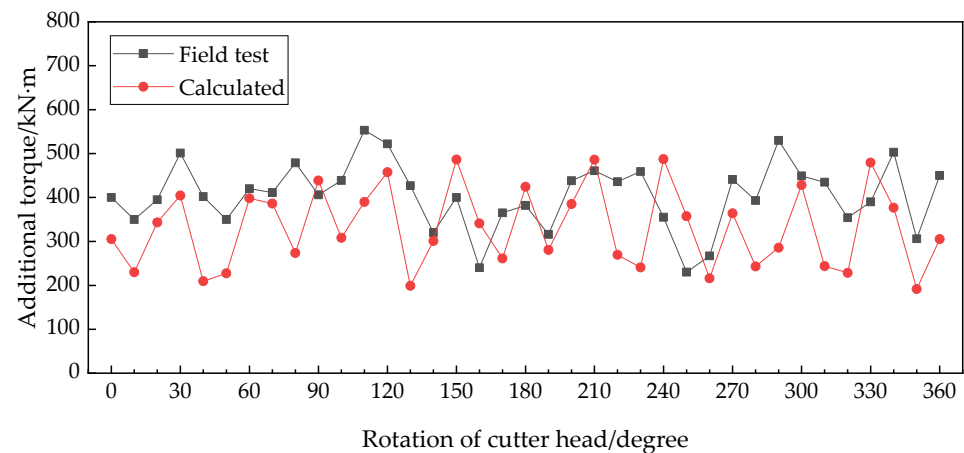


Figure 12. Additional torque in different rotation angles (pile No. 1, $B = 800$ mm, $e = 0.2 D$).

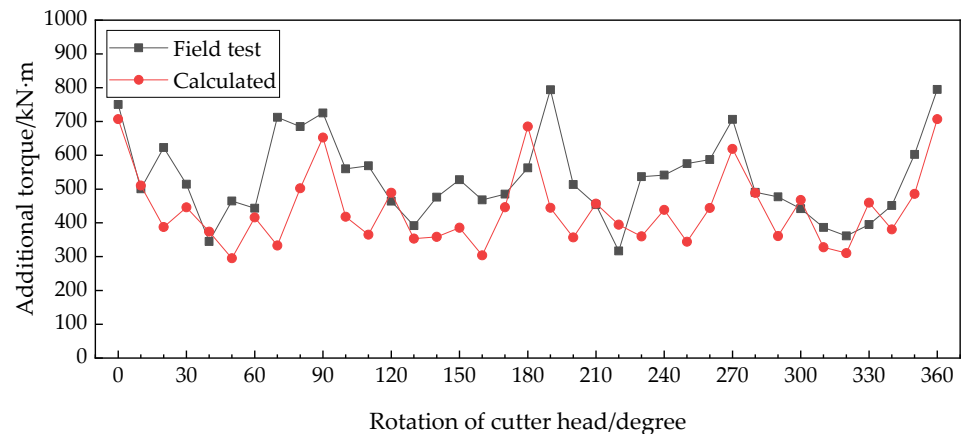


Figure 13. Additional torque with different rotation angles (pile No. 2, $B = 1200$ mm, $e = 0$).

5.2. Additional Torque at Different Cutting Distances

Additional torque at different cutting distances when cutting through pile No. 1 and pile No. 2 are shown in Figures 14 and 15, respectively. As can be seen, with the increase of cutting distance, the additional torque presents a trend of first increasing and then decreasing. The main reason is the change of the cutting area and the number of tools that are in contact with the pile. According to the calculated results, the additional torque reaches the maximum value when the cutting distance reaches the radius of pile. This agrees with the conventional mechanical analysis. Field test additional torque in Figure 14 decreases significantly when the cutting distance is half the diameter of the pile and then increases rapidly. This is caused by the operator's active adjustment of the shield tunneling state. In actual excavation process, the shield advance rate and the thrust decreased when cutting to this position. Then, the shield operator actively increased the thrust to ensure shield advancing. As the advance rate increased, the penetration of the cutter became larger, causing the rise of tools' cutting force and the total torque of the cutter head. This suggests that it is important to maintain proper thrust and lower advance rate during cutting pile process to avoid excessive cutter head torque. The additional torque predicted by the calculation model is in agreement with the field test results.

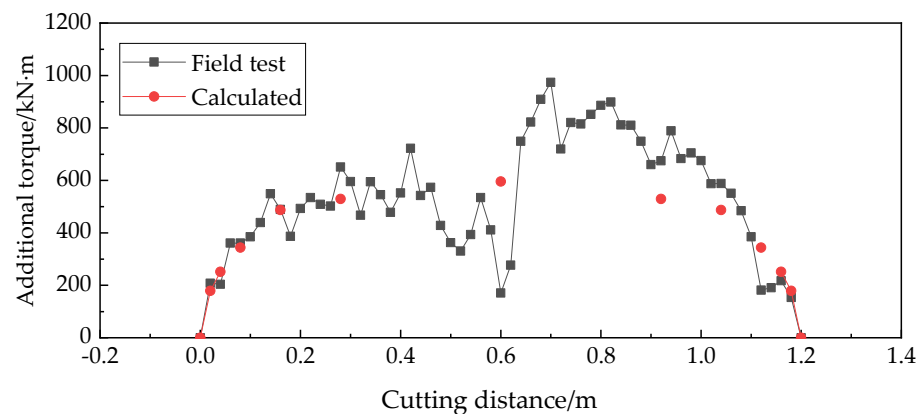


Figure 14. Additional torque at different cutting distances (pile No.1, $e = 0.2 D$).

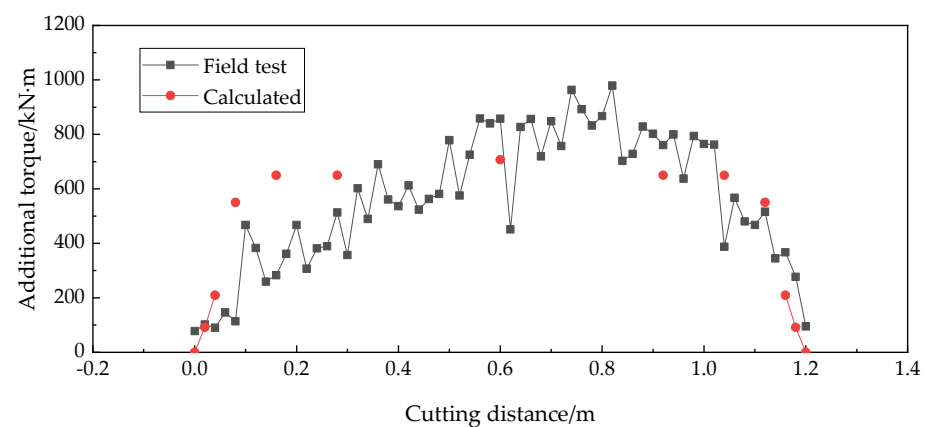


Figure 15. Additional torque at different cutting distances (pile No. 2, $e = 0$).

6. Parametric Study and Discussions

There are two important parameters in the calculation model: cutting surface width B and eccentric distance e . In engineering practice, a shield machine may need to cut several piles of different diameters or in different positions. Eccentric distance varies with the changes of the relative position of the pile and cutter head, and the interaction force between the pile and cutter head also changes. For the same circular pile, with the continuous cutting process of shield machine, the width of the cutting surface between the cutter head and pile changes constantly (from 0 to D and then to 0). In this section, the effects of the cutting surface width B and eccentric distance e on the interaction forces are discussed. It should be noted that since both forces and moments are vectors, the sign of the calculated result represents the direction in Cartesian coordinates. In order to better compare and demonstrate the variation law of force and moment under different pile cutting parameters, the force and moment in the following discussion represent their magnitude.

6.1. Effect of Cutting Surface Width

Figure 16 illustrates the relations between interaction forces F_x , F_y , F_z and cutting surface width B under different eccentric distances of 0 , $0.1 D$, $0.2 D$, $0.4 D$ and $0.6 D$, where $D = 6$ m is the diameter of the shield machine. It can be observed that with the increase of the cutting surface width, the interaction forces F_x , F_y and F_z show an overall increasing trend with slight decreases in some ranges. The main reason is the increase of the number of tools. The interaction force F_z is much greater than F_x and F_y , and increases significantly. Especially when the cutting surface width exceeds 1.0 m, the gap is more obvious. A possible reason is that when the pile foundation width is large, the tools at the opposite sides of the cutter head (upper side and lower side) have opposite cutting directions (in the X direction) and they partly cancel out cutting force of each other, while cutting forces in

the Y direction were added to each other and penetrate forces in the Z direction have the same signs as well.

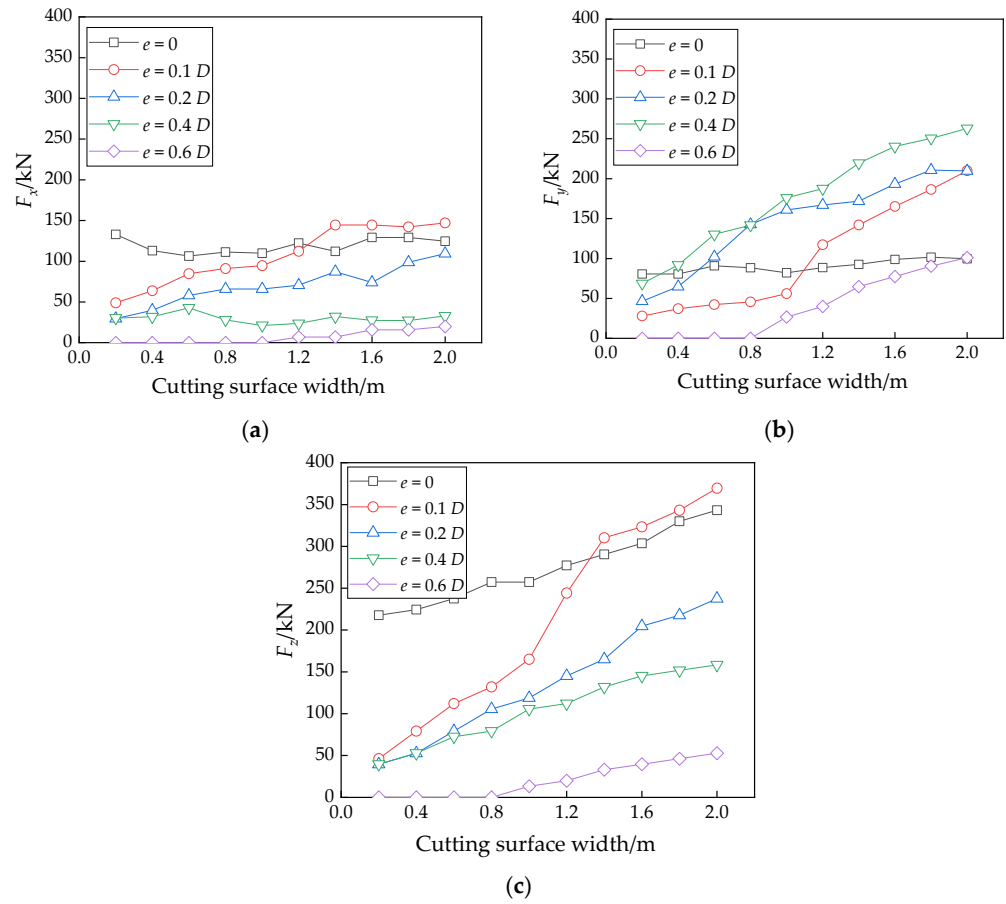


Figure 16. Effect of the cutting surface width B on the interaction forces: (a) F_x ; (b) F_y and (c) F_z .

The relations between the moments M_x , M_y , M_z and cutting surface width B under different eccentric distances are shown in Figure 17. In a similar way as the interaction force, the moments increase with the width of the cutting surface, and the moment M_z increases more significantly. M_z , which can be considered as the additional torque of the shield cutter head, is also much greater than M_x and M_y , which are considered unbalanced moments. Therefore, it can be inferred that the adequate torque for the shield machine is required to ensure that the shield can cut piles and pass through quickly.

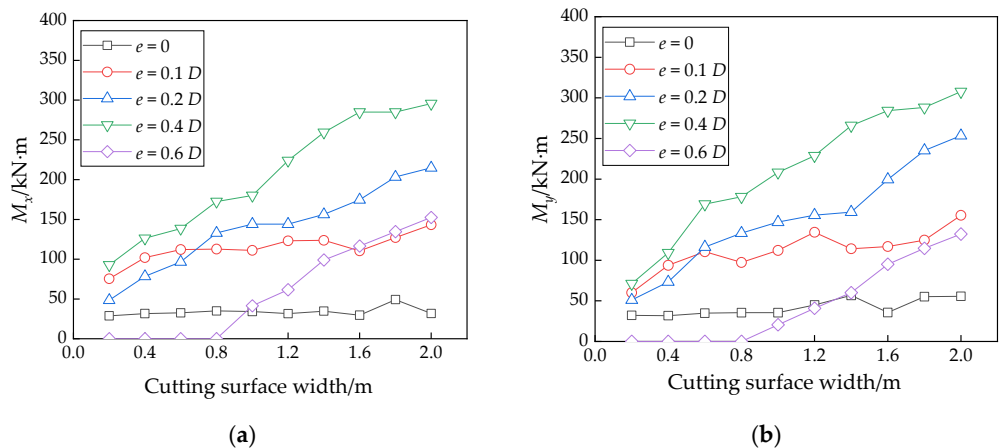


Figure 17. Cont.

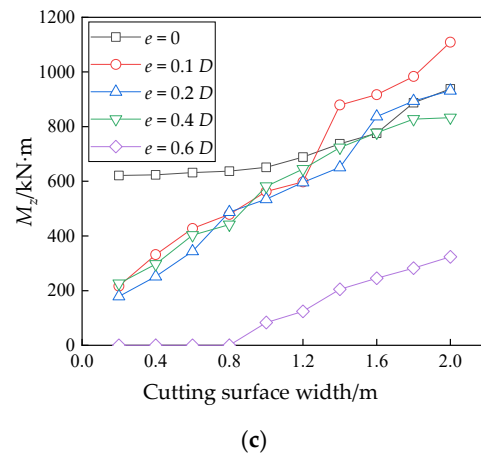


Figure 17. Effect of the cutting surface width B on the interaction moment: (a) M_x ; (b) M_y and (c) M_z .

6.2. Effect of the Eccentric Distance

Figure 18 presents the relation between interaction forces F_x, F_y, F_z and cutting surface width B under different eccentric distances of $0, 0.1 D, 0.2 D, 0.4 D$ and $0.6 D$, where $D = 6$ m is the diameter of the shield machine. As shown in Figure 18a, F_x decreases linearly with the increase of eccentric distance; the main reason for this is that the number of cutting tools reduced. The tools on opposite sides of the cutter head have different cutting directions, which cancel each other out. Therefore, the unbalance force of cutter head F_x is usually small. As shown in Figure 18b, F_y generally presents a trend of increasing first and then decreasing and reaches a peak at about $0.3 D-0.4 D$. F_y is affected by both the number of tools and the cutting force angle of the tools. On the one hand, the increase of the eccentric distance causes the cutting force component of the tools in the Y direction to increase, which thereby increases F_y . On the other hand, as the eccentric distance increases, the number of tools involved in cutting the pile decreases, which causes F_y to decrease. In engineering practice, the appropriate cutter head rotation direction can be set actively to increase the force applied on the pile, thereby reducing pile settlement and formation disturbance. As shown in Figure 18c, F_z declines overall. F_z decreases rapidly when the centrifugal distance is in the range of $0-0.1 D$ and greater than $0.4 D$ and changes smoothly when the eccentric distance is in the range of $0.1-0.4 D$. The main reason is the change in the number of tools.

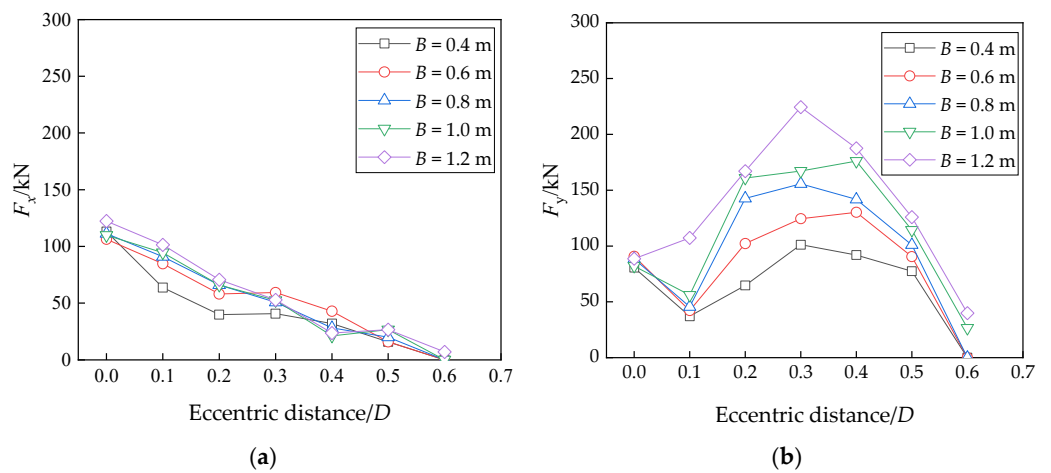


Figure 18. Cont.

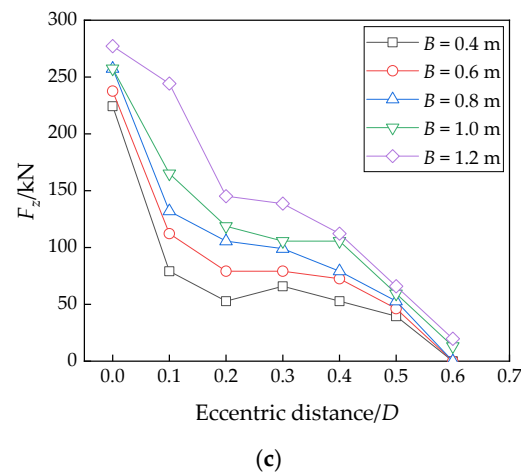


Figure 18. Effect of the eccentric distance e on the interaction forces: (a) F_x ; (b) F_y and (c) F_z .

Figure 19 presents the relation between interaction forces M_x , M_y , M_z and cutting surface width B under different eccentric distances of 0, 0.1 D , 0.2 D , 0.4 D and 0.6 D . M_x and M_y generally show a similar trend of increasing first and then decreasing, and reaches a peak at about 0.3 D –0.4 D . They reach the peaks when the eccentric distance is about 0.3 D –0.4 D . This is the result of the combined effect of the change in the number of tools, the change in the force arm and the moments in different directions. The moments caused by the tools at the opposite sides of the cutter head (upper side and lower side for M_x ; left side and right side for M_y) have different signs. Notably, the magnitude of M_z is significantly larger than that of M_x and M_y . A reason is that the cutting force of tool is usually greater than the penetration force. Another reason is that all of the moments caused by cutting force of tools have the same sign. In addition, with the increase of eccentric distance, M_z declines first, then increases, and decreases to 0 at last. The peak in the ascending interval appears at about 0.3 D –0.4 D . The main reason for this is the change in the number of tools involved.

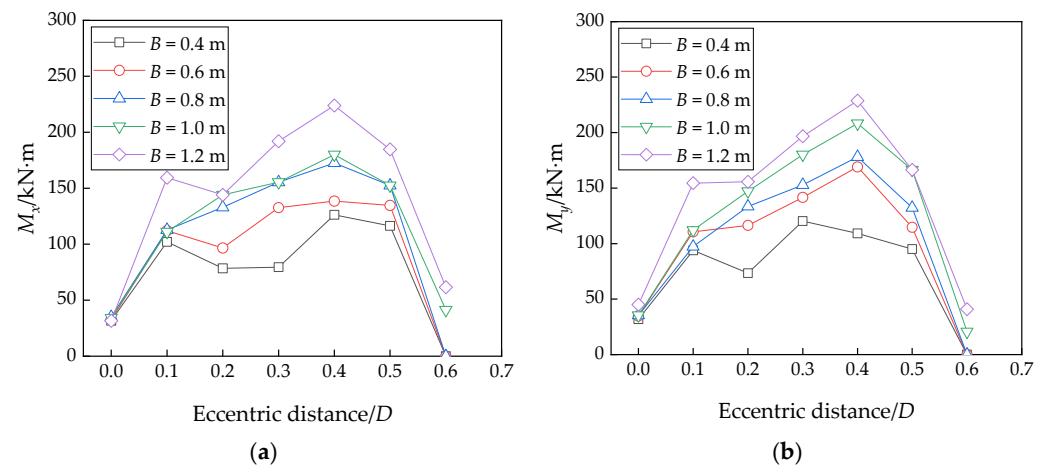


Figure 19. Cont.

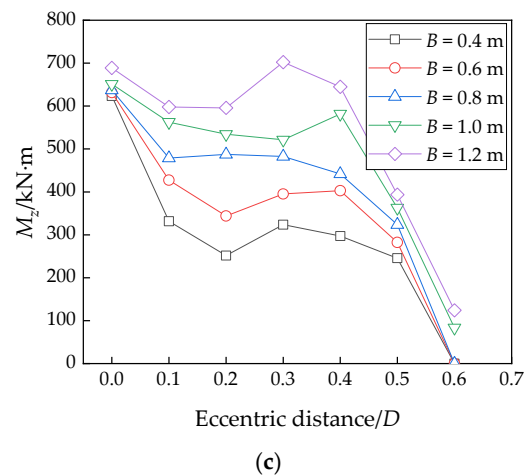


Figure 19. Effect of the eccentric distance e on the moments: (a) M_x ; (b) M_y and (c) M_z .

7. Conclusions

In order to study the interaction between the pile and shield machine in the process of cutting reinforced concrete foundation, a calculation model of the interaction force is established in this paper. A field test of cutting two piles was conducted and the rationality of the model is verified by comparing the calculation results with field test data. The model is applied in an actual cutting-pile project in Harbin, China. The shield operation parameters are predicted and compared with field test results. Besides, the effects of cutting surface width and eccentric distance on the interaction force are discussed.

- (1) The calculation and field test results show that when the shield machine cuts reinforced concrete piles, there is a significant interaction between the cutter head and the piles, which causes obvious changes in the shield operation parameters and shield performance.
- (2) The number of tools has a significant effect on the additional torque of cutter head. The additional torque fluctuates with the rotation of cutter head and increases obviously with the increase of the number of tools that are inside the cutting area. The number of these tools are also determined by the arrangement of tools, cutting surface width and eccentric distance.
- (3) As the cutting distance increases, the additional torque of cutter head shows a trend of first increasing and then decreasing and reaches the maximum value when the cutting distance reaches the radius of pile. The maximum additional torque from the field test in this paper is about 1000 kN·m. This suggests that it is important to pay close attention to the torque and ensure that there is sufficient torque reserve.
- (4) The interaction force under different cutting surface width and eccentric distance conditions are given and discussed. The penetration force in the shield tunneling direction is usually greater than the unbalanced force in the other two directions. The additional torque of cutter head rotation is usually greater than the unbalanced moments in the other two directions as well. Besides, the additional force and additional moment of the cutter head increase with the increase of the cutting surface width. The impacts of eccentric distance on additional force and additional moment are complicated.
- (5) The additional force and additional moment given in this paper can provide reference for similar engineering. The discussion of the interaction between piles and cutter head under the conditions of different cutting surface width and different eccentric distances can provide guidance for the setting of shield operation parameters in other field projects with similar tools configurations and cutting conditions. However, the data given in this article are based on specific examples of project. The specific calculation and analysis of actual engineering conditions should be considered when findings of this study are applied to different projects.

Author Contributions: Conceptualization, X.W. and D.Y.; methodology, X.W. and D.Y.; software, X.W.; validation, X.W. and D.Y.; formal analysis, X.W.; investigation, X.W. and D.Y.; resources, D.Y.; data curation, X.W.; writing—original draft preparation, X.W.; writing—review and editing, X.W. and D.Y.; visualization, X.W.; supervision, D.Y.; project administration, D.Y.; funding acquisition, D.Y. All authors have read and agreed to the published version of the manuscript.

Funding: This research was supported by the Key Project of High-speed Rail Joint Fund of the National Natural Science Foundation of China under Grant No. U1834208.

Institutional Review Board Statement: Not applicable.

Informed Consent Statement: Not applicable.

Data Availability Statement: The data presented in this study are available from the corresponding author upon request.

Acknowledgments: The authors extend their thanks to Youchao Du (CCCC First Harbour Engineering Co., Ltd.) for providing related data.

Conflicts of Interest: The authors declare no conflict of interest.

References

- Liao, S.; Liu, J.; Wang, R.; Li, Z. Shield tunneling and environment protection in Shanghai soft ground. *Tunn. Undergr. Space Technol.* **2009**, *24*, 454–465. [[CrossRef](#)]
- Su, J.; Fang, Q.; Zhang, D.; Niu, X.; Liu, X.; Jie, Y. Bridge responses induced by adjacent subway station construction using shallow tunneling method. *Adv. Civ. Eng.* **2018**, *2018*, 8918749. [[CrossRef](#)]
- Koyama, Y. Present status and technology of shield tunneling method in Japan. *Tunn. Undergr. Space Technol.* **2003**, *18*, 145–159. [[CrossRef](#)]
- Zhang, C.; Zhao, Y.; Zhang, Z.; Zhu, B. Case Study of Underground Shield Tunnels in Interchange Piles Foundation Underpinning Construction. *Appl. Sci.* **2021**, *11*, 1611. [[CrossRef](#)]
- Li, Z.; Chen, Z.; Wang, L.; Zeng, Z.; Gu, D. Numerical simulation and analysis of the pile underpinning technology used in shield tunnel crossings on bridge pile foundations. *Undergr. Space* **2021**, *6*, 396–408. [[CrossRef](#)]
- Zhang, L. Study on underpinning scheme of viaduct pile foundation crossed by shield tunnel. *IOP Conf. Ser. Earth Environ. Sci.* **2020**, *570*, 052028. [[CrossRef](#)]
- Selemetas, D.; Standing, J.; Zdravković, L. Response of full-scale piles to EPBM tunnelling in London Clay. *Géotechnique* **2017**, *67*, 823–836. [[CrossRef](#)]
- Iwasaki, Y.; Watanabe, H.; Fukuda, M.; Hirata, A.; Hori, Y. Construction control for underpinning piles and their behaviour. *Geotechnique* **1994**, *44*, 681–689. [[CrossRef](#)]
- Wang, Y.; Wang, X.; Xiong, Y.; Yang, Z.; Zhang, J. Full-Scale Laboratory Test of Cutting Large-Diameter Piles Directly by Shield Cutterhead. *Adv. Civ. Eng.* **2022**, *12*, 1–11. [[CrossRef](#)]
- Xu, Q.; Zhu, H.; Ma, X.; Ma, Z.; Li, X.; Tang, Z.; Zhuo, Z. A case history of shield tunnel crossing through group pile foundation of a road bridge with pile underpinning technologies in Shanghai. *Tunn. Undergr. Space Technol.* **2015**, *45*, 20–33. [[CrossRef](#)]
- Chen, L.; Poulos, H.; Loganathan, N. Pile responses caused by tunneling. *J. Geotech. Geoenviron.* **1999**, *125*, 207. [[CrossRef](#)]
- Huang, M.; Zhang, C.; Li, Z. A simplified analysis method for the influence of tunneling on grouped piles. *Tunn. Undergr. Space Technol.* **2009**, *24*, 410–422. [[CrossRef](#)]
- Xiang, Y.; Feng, S. Theoretical prediction of the potential plastic zone of shallow tunneling in vicinity of pile foundation in soils. *Tunn. Undergr. Space Technol.* **2013**, *38*, 115–121. [[CrossRef](#)]
- Marshall, A. Tunnel-Pile Interaction Analysis Using Cavity Expansion Methods. *J. Geotech. Geoenviron.* **2012**, *138*, 1237–1246. [[CrossRef](#)]
- Marshall, A.; Haji, T. An analytical study of tunnel–pile interaction. *Tunn. Undergr. Space Technol.* **2015**, *45*, 43–51. [[CrossRef](#)]
- Franza, A.; Marshall, A.; Haji, T.; Abdelatif, A.; Carbonari, S.; Morici, M. A simplified elastic analysis of tunnel-piled structure interaction. *Tunn. Undergr. Space Technol.* **2017**, *61*, 104–121. [[CrossRef](#)]
- Zhang, Z.; Huang, M.; Xu, C.; Jiang, Y.; Wang, W. Simplified solution for tunnel-soil-pile interaction in Pasternak’s foundation model. *Tunn. Undergr. Space Technol.* **2018**, *78*, 146–158. [[CrossRef](#)]
- Afifipour, M.; Sharifzadeh, M.; Shahriar, K.; Jamshidi, H. Interaction of twin tunnels and shallow foundation at Zand underpass, Shiraz metro, Iran. *Tunn. Undergr. Space Technol.* **2011**, *26*, 356–363. [[CrossRef](#)]
- Jongpradist, P.; Kaewsri, T.; Sawatparnich, A.; Suwansawat, S.; Youwai, S.; Kongkitkul, W.; Sunitsakul, J. Development of tunneling influence zones for adjacent pile foundations by numerical analyses. *Tunn. Undergr. Space Technol.* **2013**, *34*, 96–109. [[CrossRef](#)]
- Hong, Y.; Soomro, M.; Ng, C.W. Settlement and load transfer mechanism of pile group due to side-by-side twin tunnelling. *Comput. Geotech.* **2015**, *64*, 105–119. [[CrossRef](#)]

21. Li, Y.; Zhang, W. Investigation on passive pile responses subject to adjacent tunnelling in anisotropic clay. *Comput. Geotech.* **2020**, *127*, 103782. [[CrossRef](#)]
22. Fu, J.; Yang, J.; Zhu, S.; Shi, Y. Performance of Jet-Grouted Partition Walls in Mitigating the Effects of Shield-Tunnel Construction on Adjacent Piled Structures. *J. Perform. Constr. Fac.* **2017**, *31*, 04016096. [[CrossRef](#)]
23. Kong, S.; Oh, D.; Lee, S.; Kim, C.; Lee, Y. Effects of Pile Installation on Existing Tunnels Using Model Test and Numerical Analysis with Medium Density Sand. *Appl. Sci.* **2021**, *11*, 6904. [[CrossRef](#)]
24. Loganathan, N.; Poulos, H.; Stewart, D. Centrifuge model testing of tunnelling-induced ground and pile deformations. *Géotechnique* **2000**, *50*, 283–294. [[CrossRef](#)]
25. Jacobsz, S.; Standing, J.; Mair, R.; Hagiwara, T.; Sugiyama, T. Centrifuge modelling of tunnelling near driven piles. *Soils Found.* **2004**, *44*, 49–56. [[CrossRef](#)]
26. Chiang, K.; Lee, C. Responses of single piles to tunneling-induced soil movements in sandy ground. *Can. Geotech. J.* **2007**, *44*, 1224–1241. [[CrossRef](#)]
27. Marshall, A.; Robert, J. Tunneling beneath driven or jacked end-bearing piles in sand. *Can. Geotech. J.* **2011**, *48*, 1757–1771. [[CrossRef](#)]
28. Ng, C.; Hu, L.; Peng, S. Three-dimensional centrifuge modelling of the effects of twin tunnelling on an existing pile. *Tunn. Undergr. Space Technol.* **2013**, *35*, 189–199. [[CrossRef](#)]
29. Ng, C.; Mukhtiar, A.; Yi, H. Three-dimensional centrifuge modelling of pile group responses to side-by-side twin tunnelling. *Tunn. Undergr. Space Technol.* **2014**, *43*, 350–361. [[CrossRef](#)]
30. Franza, A.; Marshall, A. Centrifuge modeling study of the response of piled structures to tunneling. *J. Geotech. Geoenviron.* **2018**, *144*, 04017109. [[CrossRef](#)]
31. Lee, Y.; Richard, H. Influence zones for 2D pile–soil–tunnelling interaction based on model test and numerical analysis. *Tunn. Undergr. Space Technol.* **2007**, *22*, 325–342. [[CrossRef](#)]
32. Meguid, M.; Joe, M. Investigation of tunnel-soil-pile interaction in cohesive soils. *J. Geotech. Geoenviron.* **2009**, *135*, 973–979. [[CrossRef](#)]
33. Deng, L.; Yuan, Y.; Zhuang, Q.; Li, X.; Zhang, C.; Li, W. Novel PDC cutter for reinforced concrete based on linear and rotational cutting tests. *Tunn. Undergr. Space Technol.* **2022**, *129*, 104681. [[CrossRef](#)]
34. Yuan, D.; Wang, F.; Dong, C.; Han, B.; Wang, M. Study on new-style cutter for shield cutting large-diameter reinforced concrete pile. *China J. Highw. Transp.* **2016**, *29*, 89. (In Chinese) [[CrossRef](#)]
35. Wang, F.; Yuan, D.; Dong, C.; Han, B.; Nan, H.; Wang, M. Study on cutter configuration for directly shield cutting of large-diameter piles. *China Civ. Eng. J.* **2013**, *46*, 127–135. (In Chinese) [[CrossRef](#)]
36. Copur, H.; Bilgin, N.; Balci, C.; Tumac, D.; Avunduk, E. Effects of Different Cutting Patterns and Experimental Conditions on the Performance of a Conical Drag Tool. *Rock Mech. Rock Eng.* **2017**, *5*, 1585–1609. [[CrossRef](#)]
37. Banadaki, M.; Mohanty, B. Numerical simulation of stress wave induced fractures in rock. *Int. J. Impact Eng.* **2012**, *40*, 16–25. [[CrossRef](#)]
38. Xu, Y.; Li, X.; Yang, Y.; Mu, J.; Su, W. Dynamic response test of shield cutter in the process of cutting concrete. *J. Harbin Inst. Technol.* **2021**, *53*, 182–189. (In Chinese) [[CrossRef](#)]
39. Xu, P.; Zuo, S. Study on the JH-2 Model Parameters for Metro Shield Cutting Reinforced Concrete Pile. *Geotech. Geol. Eng.* **2021**, *39*, 5267–5278. [[CrossRef](#)]
40. Su, W.; Li, X.; Xu, Y.; Jin, D. Numerical simulation of shield tool cutting concrete based on HJC model. *J. Zhejiang Univ. Eng. Sci.* **2020**, *54*, 1106–1114. (In Chinese) [[CrossRef](#)]

Disclaimer/Publisher’s Note: The statements, opinions and data contained in all publications are solely those of the individual author(s) and contributor(s) and not of MDPI and/or the editor(s). MDPI and/or the editor(s) disclaim responsibility for any injury to people or property resulting from any ideas, methods, instructions or products referred to in the content.